JOURNAL OF GUIDANCE, CONTROL, AND DYNAMICS
Vol. 26, No. 3, May–June 2003

Periodic Solutions in Electrodynamic Tethers on Inclined Orbits

J. Peláez*
Universidad Politécnica de Madrid, E-28040 Madrid, Spain
and
M. Lara†
Real Observatorio de la Armada, E-11110 San Fernando, Spain

A new kind of dynamic instability affecting electrodynamic tethers flying in inclined orbits has been recently investigated. After assuming a rigid tether model, a nontilted dipole model for the Earth magnetic field, and a constant tether current, the system governing equations are forced by electromagnetic terms with orbital period. The orbital inclination i and the nondimensional ratio ε_1 between the magnitude of the electrodynamic forces acting on the tether and the vertical gravity gradient are the leading parameters in the model. When $\varepsilon_1 = 0$, the system has a sole stable equilibrium position with the tether aligned with the local vertical. When $\varepsilon_1 \neq 0$, the governing equations have periodic solutions with orbital period because of the frequency entrainment with the forcing terms. There is a special periodic solution that plays an important role in the analysis and that reduces to the stable equilibrium position when $\varepsilon_1 \to 0$. Previous analysis of the nonlinear equations have been made by using asymptotic techniques in the limit $\varepsilon_1 \to 0$. In this paper we introduce an algorithm based on the Poincaré method of continuation of periodic orbits, which allows the extension of the analysis to values of ε_1 of order unity. This algorithm also leads to other periodic solutions that cannot be uncovered by using asymptotic techniques. Unfortunately, these other periodic solutions exhibit a stronger unstable behavior than the first family of solutions, and they are not suitable for the operation of an electrodynamic tether.

Nomenclature

A_θ	=	amplitude of the θ oscillation, nondimensional
A_φ	=	amplitude of the φ oscillation, nondimensional
a	=	radius of the center of mass circular orbit, km
cn	=	Jacobian elliptic function
emf	=	voltage drop between the two tether ends, V
$\boldsymbol{F}$	=	vector field of a dynamical system
f_e	=	electrodynamic torque factor, defined in Eq. (19)
$\boldsymbol{I}$	=	$n \times n$ identity matrix
I_m	=	tether current averaged over the total length, A
$I(s)$	=	current distribution along the tether, A
i	=	orbital inclination, deg
j	=	imaginary number
$K(\,)$	=	complete elliptic integral of the first kind
k	=	stability index of a periodic orbit
L	=	tether length, km
m	=	tether mass, kg
m_B	=	mass of the endmass, kg
n_∞	=	ionospheric plasma density, m^{-3}
O	=	center of mass; origin on the orbital frame
s	=	distance from the orbiter end O, m
sn	=	Jacobian elliptic function
T	=	period of an orbit, s
t	=	time, s
$\boldsymbol{x}$	=	vector state of a dynamical system
α	=	$\pi\sqrt{3}$, appears in Eq. (27)
ε	=	electrodynamic parameter, defined in Eq. (18)
ε_1	=	electrodynamic parameter, defined in Eq. (1)
θ	=	tether in-plane angle, rad
λ	=	eigenvalues of the monodromy matrix
μ	=	Earth's gravitational constant, km^3/s^2
μ_m	=	magnetic moment of the Earth's dipole, $T \cdot km^3$
ν	=	true anomaly of the orbit of O, rad
ν_θ	=	phase of the θ oscillation, nondimensional
ν_φ	=	phase of the φ oscillation, nondimensional
ν_0	=	initial true anomaly, rad
$\boldsymbol{\xi}$	=	initial conditions of a orbit
σ	=	free parameter of a dynamical system and true anomaly in the unperturbed problem
φ	=	tether out-of-plane angle, rad
ω	=	angular frequency of the orbit, s^{-1}
$(\dot{})$	=	$d(\,)/d\nu$ or $d(\,)/dt$

Received 8 August 2001; revision received 14 May 2002; accepted for publication 14 January 2003. Copyright © 2003 by the American Institute of Aeronautics and Astronautics, Inc. All rights reserved. Copies of this paper may be made for personal or internal use, on condition that the copier pay the $10.00 per-copy fee to the Copyright Clearance Center, Inc., 222 Rosewood Drive, Danvers, MA 01923; include the code 0731-5090/03 $10.00 in correspondence with the CCC.

*Associate Professor, E.T.S.I. Aeronáuticos, Pza. Cardenal Cisneros 3; jpelaez@faia.upm.es.
†Commander, Spanish Navy, Cecilio Pujazón s/n, Cádiz; mlara@roa.es.

Introduction

ELECTRODYNAMIC tethers[1–4] are among the leading applications of tethers in space transportation. Nowadays, we witness a renewed interest in their capabilities, which is based on their potential utilization in present or near future missions. For example, the main goal of the Propulsive SEDS (ProSEDS) mission,[5,6] scheduled to fly in the spring of 2003, is to check the validity of the bare tether concept. An electrodynamic bare tether will be used in the generator mode to produce electrodynamic drag with the primary goal of reentering a Delta-II second stage quickly from orbit. The use of an electrodynamic tether as thruster[7,8] has also been proposed in several scenarios.

Dynamics simulations of electrodynamic tethers on circular and inclined orbits show a very complex motion driven by the electrodynamic forces acting on the conductive tether. These forces depend on the current flowing in the wire, the tether characteristics—material, diameter, and so on—the Earth magnetic field, the ionospheric plasma density, the orbital velocity, and the tether orientation. They drive the in-plane and out-of-plane motions of the tethered system. For flexible tethers the system equilibrium positions can be unstable, as Levin[9] Beletskii and Levin[10] have shown (see Ref. 9 and also Ref. 10, pp. 268–322).

However, a new kind of dynamic instability[11–13] has been recently pointed out for electrodynamic tethers, which is independent of the tether flexibility. In Refs. 11 and 12 a simple model has been used to describe the dynamic effects of the electrodynamic forces. The tether is modeled as a rigid rod with point masses at the ends. The orbiter

mass is assumed very large with respect to the rest of the system, and the orbital decay is neglected. A nontilted dipole model for the Earth magnetic field and a constant tether current are assumed. The system dynamics equations are forced by the electromagnetic terms, which, in a first approximation, change periodically with the orbital period. The strength of the forcing terms is given by the nondimensional parameter ε_1 defined[11,12] as

$$\varepsilon_1 = \frac{3 f_e I_m}{m + 3m_B} \cdot \frac{\mu_m}{\mu} \cdot \sin i \tag{1}$$

When the current is null ($\varepsilon_1 = 0$), the system has one stable equilibrium position with the tether aligned along the local vertical. When the current is different from zero, the governing equations have no stationary solutions. However, they have periodic solutions. Because of the well-known frequency entrainment phenomenon, typical of this kind of forced systems (see Ref. 14, pp. 186–203), any periodic solution has the same period, or an integer multiple, as the forcing terms of the governing equations, that is, in this model, the orbital period. There is a special periodic solution that reduces to the stable equilibrium position when $\varepsilon_1 \to 0$, which plays an important role in the analysis.

The nonlinear analysis performed in Refs. 11 and 12 shows that, within the limitations of the model, this periodic solution is unstable for all values of the free parameters ε_1 and i. The physical reason for the instability is that, in the long term, the electrodynamic forces pump energy continually into the system. The net energy increase per orbit for the periodic solution (or state space trajectory) is zero. However, any nonperiodic trajectory in its neighborhood has a complex behavior with two stages of evolution. The total energy of the system undergoes quasi-periodic changes until it reaches a threshold beyond which the energy starts to grow without bound, with a positive net energy flux per orbit. Eventually, after several orbits the in-plane libration becomes a rotation. The mechanism responsible for this instability depends on ε_1 and i. Unlike other destabilizing mechanisms found in electrodynamic tethers, this one is present in any kind of tether system with either a flexible or a rigid tether, operating in the generator or thruster mode and utilizing a bare tether or a large spherical termination to collect the ionospheric electrons. Moreover, the mechanism (but not the growth rate of the instability) is independent of the presence of additional resonant force components that can be generated by the magnetic and plasma fields.

In Refs. 11 and 12 asymptotic techniques have been used to obtain, in the limit $\varepsilon_1 \to 0$, 1) the family of periodic solutions and 2) the monodromy matrix of their variational equations with the moduli of its eigenvalues, which give the stability properties of the system. That analysis holds for small values of ε_1, the parameter of the family, but it is no longer valid when ε_1 is of order unity. In such a case a different mathematical approach is required. In this paper we describe briefly a numeric algorithm based on the Poincaré method of continuation of periodic orbits,[15] and we use it to extend the analysis of Refs. 11 and 12 to cases in which the parameter ε_1 is of order unity.

As part of its output, the numeric algorithm gives the stability properties of any periodic solution that it finds. It also permits to use either ε_1 or i as the family parameter of the periodic solutions as well. This way we can describe the evolution of the stability properties with the orbital inclination i for any given value of ε_1. Apart from the special periodic solution studied in Refs. 11 and 12, the governing equations have additional periodic solutions that cannot be detected with asymptotic techniques. The algorithm provides these additional periodic solutions and their stability properties.

The analysis would be extended to study other interesting situations. For example, the day–night cycle on the plasma density can be modeled with an harmonic function with the same period of the orbit. In the same way the intensity of the current mainly depends on the ionospheric plasma density n_∞ and the voltage drop between the two ends of the conductive tether generated by the Earth's magnetic field(emf). Assuming, in approximation, a constant emf, the current exhibits a dependence (latitudinal dependence) with n_∞ that can be modeled with an harmonic component at twice the orbital frequency. Both cases could be analyzed introducing a time dependence on the parameter ε_1. In the first case $\varepsilon_1 = \varepsilon_0[1 + \delta \cos(\omega t + \psi)]$ and in the second $\varepsilon_1 = \varepsilon_0[1 + \delta \cos(2\omega t + \psi)]$. Its effects on the stability properties of the system can be obtained with the same procedure we use here; the study is in progress, and results will be soon presented.

Numeric Algorithm

In this section we present the fundamentals of the numerical algorithm. Differential correction algorithms are frequently used for the numerical computation of periodic orbits of conservative dynamical systems. References 16–19 or the more recent[20,21] can be cited among many others.

The algorithm used in this paper is based on the Poincaré's continuation method of periodic solutions. A full description of the Poincaré's method can be found in Ref. 15. More details on the algorithm are given in Refs. 22 and 23.

Let

$$\dot{\boldsymbol{x}} = \boldsymbol{F}(\boldsymbol{x}; \sigma) \tag{2}$$

be an autonomous system of n differential equations depending on a parameter σ. Any solution

$$\boldsymbol{x} = \boldsymbol{x}(t; \boldsymbol{\xi}; \sigma) \tag{3}$$

of Eq. (2) is a function of the parameter σ and the initial conditions $\boldsymbol{\xi} = \boldsymbol{x}(0; \boldsymbol{\xi}; \sigma)$. Let us suppose that, for a given value $\sigma = \sigma_0$ of the parameter and for the initial conditions $\boldsymbol{\xi} = \boldsymbol{\xi}_0$, a periodic solution of system (2)

$$\boldsymbol{x}(t; \boldsymbol{\xi}_0; \sigma_0) = \boldsymbol{x}(t + T_0; \boldsymbol{\xi}_0; \sigma_0) \tag{4}$$

with period $T_0 > 0$ is known. The Poincaré's continuation method deals with the problem of computing the analytic continuation of Eq. (4) for values of the parameter close to the starting value σ_0. That is, for $\sigma = \sigma_0 + \Delta\sigma$ new initial conditions $\boldsymbol{\xi} = \boldsymbol{\xi}_0 + \Delta\boldsymbol{\xi}$ and period $T = T_0 + \Delta T$ are required to produce a new periodic solution of Eq. (2).

As a consequence of the uniqueness theorem for differential equations, Eq. (4) will hold for all t as it does for a value t_0, say, $t_0 = 0$. Therefore, the new solution shall verify the periodicity condition

$$\boldsymbol{x}(T; \boldsymbol{\xi}; \sigma) - \boldsymbol{\xi} = \boldsymbol{0} \tag{5}$$

where the existence of the implicit functions $\boldsymbol{\xi}$ is directly related to the nonvanishing of the Jacobian determinat of the left-hand side of Eq. (5). With regards to this Jacobian, there are different possibilities that depend on the existence of integrals of Eq. (2). The interested reader is referred to Ref. 15.

Rewriting Eq. (5) as

$$\boldsymbol{x}(T_0 + \Delta T; \boldsymbol{\xi}_0 + \Delta\boldsymbol{\xi}; \sigma_0 + \Delta\sigma) - (\boldsymbol{\xi}_0 + \Delta\boldsymbol{\xi}) = \boldsymbol{0} \tag{6}$$

and expanding it around $(T_0; \boldsymbol{\xi}_0; \sigma_0)$ to the first order, it yields the linear system

$$(\boldsymbol{\nabla}_{\xi}\boldsymbol{x} - \boldsymbol{I}) \cdot \Delta\boldsymbol{\xi} + \boldsymbol{F}(\boldsymbol{x}; \sigma_0)\,\Delta T + \frac{\partial \boldsymbol{x}}{\partial \sigma}\Delta\sigma = -(\boldsymbol{x} - \boldsymbol{\xi}_0) \tag{7}$$

that must be computed at $(T_0; \boldsymbol{\xi}_0; \sigma_0)$ and where $\boldsymbol{I}$ is the $n \times n$ identity matrix.

Equation (7) provides the basic scheme for implementing the Poincaré's continuation method. For a periodic solution of Eq. (2), the right-hand side of Eq. (7) vanishes because of Eq. (4), and the linear system

$$(\boldsymbol{\nabla}_{\xi}\boldsymbol{x} - \boldsymbol{I}) \cdot \frac{\Delta\boldsymbol{\xi}}{\Delta\sigma} + \boldsymbol{F}(\boldsymbol{x}; \sigma_0)\frac{\Delta T}{\Delta\sigma} = -\frac{\partial \boldsymbol{x}}{\partial \sigma} \tag{8}$$

at $(T_0; \boldsymbol{\xi}_0; \sigma_0)$ can be used to compute the initial conditions $\boldsymbol{\xi}_1 = \boldsymbol{\xi}_0 + \Delta\boldsymbol{\xi}$ and period $T_1 = T_0 + \Delta T$ of the new periodic solution of Eq. (2) corresponding to the value $\sigma_1 = \sigma_0 + \Delta\sigma$ of the parameter. Equations (8) are a tangent prediction, and, usually, they yield a new solution that is not exactly periodic, that is, $\boldsymbol{x}(T_1; \boldsymbol{\xi}_1; \sigma_1) - \boldsymbol{\xi}_1 \neq \boldsymbol{0}$.

In such a case new corrections $\Delta\boldsymbol{\xi}_1$ and ΔT_1 should be computed in order to satisfy the periodicity condition

$$\boldsymbol{x}(T_1 + \Delta T_1; \boldsymbol{\xi}_1 + \Delta\boldsymbol{\xi}_1; \sigma_1) - (\boldsymbol{\xi}_1 + \Delta\boldsymbol{\xi}_1) = \boldsymbol{0} \tag{9}$$

Equations (9) are formally equal to Eq. (6)—now with $\Delta\sigma \equiv 0$—so we can use again Eq. (7) to obtain the corrections. Then, iterative corrections could be in order from

$$(\nabla_{\xi}\boldsymbol{x} - \boldsymbol{I}) \cdot \Delta\boldsymbol{\xi}_i + \boldsymbol{F}(\boldsymbol{x}; \sigma_1)\, \Delta T_i = -(\boldsymbol{x} - \boldsymbol{\xi}_i) \tag{10}$$

evaluated at $(T_i; \boldsymbol{\xi}_i; \sigma_1)$. However, now the right-hand side no longer vanishes.

The partial derivatives of $\boldsymbol{x}$ with respect to the initial conditions $\boldsymbol{\xi}$ are computed from the homogeneous variational system

$$\nabla_{\xi}\dot{\boldsymbol{x}} = (\nabla_x \boldsymbol{F}) \cdot (\nabla_{\xi}\boldsymbol{x}) \tag{11}$$

starting from the initial conditions

$$(\nabla_{\xi}\boldsymbol{x})_{t=0} = \boldsymbol{I} \tag{12}$$

that follows from $\boldsymbol{x}(0; \boldsymbol{\xi}; \sigma) = \boldsymbol{\xi}$. Analogously, the partial derivative $\partial\boldsymbol{x}/\partial\sigma$ is a particular solution of the variational equations

$$\frac{\mathrm{d}}{\mathrm{d}t}\left(\frac{\partial \boldsymbol{x}}{\partial \sigma}\right) = (\nabla_x \boldsymbol{F}) \cdot \frac{\partial \boldsymbol{x}}{\partial \sigma} + \frac{\partial \boldsymbol{F}}{\partial \sigma} \tag{13}$$

starting from the initial conditions:

$$\left(\frac{\partial \boldsymbol{x}}{\partial \sigma}\right)_{t=0} = \boldsymbol{0} \tag{14}$$

Equations (8) and (10) provide a predictor–corrector scheme for computing the analytic continuation of Eq. (4). They turn out to be a linear systems of n equations in $n+1$ unknowns both. To solve them, one possibility is to look for new periodic orbits of the family with the same period ($\Delta T = 0$). However, these new periodic solutions do not exist in general. The normal procedure is to fix one of the initial conditions and vary the period.[24] In fact, a tangent displacement is a translation along the initial solution, which does not provide new periodic solutions. This situation can be avoided by constraining the variation of the initial conditions to lie on a $(n-1)$-dimensional manifold, usually an hyperplane, which is not tangent to the solution at $\boldsymbol{\xi}_0$.

The preceding algorithm has been successfully applied in Ref. 25. The algorithm is completely analytic, and it does not rely upon possible symmetries of the dynamical system.

Finally, note that the procedure is directly applicable to any nonautonomous system

$$\dot{\boldsymbol{x}} = \boldsymbol{F}(t; \boldsymbol{x}; \sigma) \tag{15}$$

when $\boldsymbol{F}$ depends on the independent variable t through periodic functions. The Poincaré method of continuation of periodic orbits was used by Poincaré himself in this kind of cases (see Ref. 15, p. 145).

When $\boldsymbol{F}$ depends on time, Eq. (15) could be transformed into an autonomous system at the cost of increasing the order by one unit. In the general case, this does not yield any advantage in the search for periodic solutions. However, when the right-hand side $\boldsymbol{F}(t; \boldsymbol{x}; \sigma)$ is periodic in t, it is possible to define a surface Σ, which is a global cross section for the flow of the augmented system, and to establish a Poincaré map in Σ with the same period as $\boldsymbol{F}(t; \boldsymbol{x}; \sigma)$. The fixed points of such a map correspond to the periodic solutions of the governing equations. The Poincaré method rests on this map, and this is, in essence, the reason for why the algorithm also works in those cases (more details can be found in Ref. 26, pp. 25 and 26).

In those cases the right-hand side $\boldsymbol{F}$ and the periodic solution have the same period. This is exactly the case we deal with in this paper [see Eqs. (16) and (17)]. Therefore, $\Delta T \equiv 0$, and the predictor simplifies to

$$(\nabla_{\xi}\boldsymbol{x} - \boldsymbol{I}) \cdot \frac{\Delta\boldsymbol{\xi}}{\Delta\sigma} = -\frac{\partial \boldsymbol{x}}{\partial \sigma}$$

and the corrector is

$$(\nabla_{\xi}\boldsymbol{x} - \boldsymbol{I}) \cdot \Delta\boldsymbol{\xi}_i = -(\boldsymbol{x} - \boldsymbol{\xi}_i)$$

Tether Governing Equations

We use the dynamics model described in Refs. 11 and 12. The orbital frame $Oxyz$ has the origin placed at the orbiter, the Ox axis is along the local vertical pointing to the zenith, the Oz axis is directed along the velocity vector, and the Oy axis normal to the orbital plane. The position of the rigid tether in the frame $Oxyz$ is determined by the angles φ, between the tether and the orbital plane, and θ, between the tether projection onto the orbital plane and the Ox axis. The time evolution of both angles is governed by the equations

$$\ddot{\theta} - 2(1+\dot{\theta})\dot{\varphi}\tan\varphi + \tfrac{3}{2}\sin 2\theta = -\varepsilon \sin i \times [\tan\varphi(2\sin\nu\cos\theta - \cos\nu\sin\theta) + \cot i] \tag{16}$$

$$\ddot{\varphi} + \sin\varphi\cos\varphi[(1+\dot{\theta})^2 + 3\cos^2\theta] = \varepsilon \sin i \times (2\sin\nu\sin\theta + \cos\nu\cos\theta) \tag{17}$$

where a dot means derivative with respect to the true anomaly ν, measured from the line of nodes ($\nu = \nu_0 + \omega t$). The tether current is on at the initial time ($t = 0$). Instead of the parameter ε_1 of Refs. 11 and 12, which is appropriate for the asymptotic analysis, we use a new parameter ε, which decouples the effects of the inclination and the electrodynamic forces. Both parameters are related by the equation

$$\varepsilon_1 = \varepsilon \cdot \sin i \Leftrightarrow \varepsilon = \frac{3 f_e I_m}{m + 3m_B} \cdot \frac{\mu_m}{\mu} \tag{18}$$

As a consequence, the dependence of the system dynamics on the orbital inclination becomes clearer. The numeric factor f_e permits a convenient formulation of the electrodynamic torques acting on the system that is valid for a generic distribution of the current along the tether. The current and f_e are given by the formulas

$$I_m = \frac{1}{L}\int_0^L I(s)\,\mathrm{d}s, \qquad f_e I_m L^2 = \int_0^L sI(s)\,\mathrm{d}s \tag{19}$$

Note that $f_e = \frac{1}{2}$ for a uniform current in the wire. For the generator mode $I_m > 0$, and for the thruster mode $I_m < 0$.

When the tether current is null, Eqs. (16) and (17) become

$$\ddot{\theta} - 2(1+\dot{\theta})\dot{\varphi}\tan\varphi + \tfrac{3}{2}\sin 2\theta = 0 \tag{20}$$

$$\ddot{\varphi} + \sin\varphi\cos\varphi[(1+\dot{\theta})^2 + 3\cos^2\theta] = 0 \tag{21}$$

These equations describe the dynamics of the unperturbed system.

To obtain the time evolution of the system, Eqs. (16) and (17) [or Eqs. (20) and (21)] must be integrated from given initial conditions at

$$\nu = \nu_0: \quad \theta = \theta_0, \qquad \varphi = \varphi_0, \qquad \dot{\theta} = \dot{\theta}_0, \qquad \dot{\varphi} = \dot{\varphi}_0 \tag{22}$$

The interested reader will find more details about this approach in Refs. 11 and 12.

Periodic Solutions

When $\varepsilon = 0$, that is, when there is no current in the tether, the system is Hamiltonian, and Eqs. (20) and (21) show several equilibrium positions:

1) $\theta = 0$, $\varphi = 0$: The tether is aligned along the local vertical pointing to the zenith.

2) $\theta = \pi$, $\varphi = 0$: The tether is aligned along the local vertical pointing to the nadir.

3) $\theta = \pm\pi/2, \varphi = 0$: The tether lies on the tangent to the orbit.

4) $\varphi = \pm\pi/2$ and θ arbitrary: The tether is normal to the orbital plane.

The equilibrium positions 3) and 4) are unstable, whereas 1) and 2) are stable. From the point of view of the operation of an electrodynamic tether, the positions 3) and 4) have an additional, and important, drawback: the current collected in the wire is very small because the voltage drop across the tether, emf, generated by the Earth magnetic field is very small. For this reason we begin our study considering the stable equilibrium positions 1) and 2). In fact, we only study the equilibrium position 1) because the analysis of the position 2) can be obtained from the analysis of 1) by replacing θ for $\theta + \pi$ and ε for $-\varepsilon$.

The 2π-periodic solutions of the unperturbed system [Eqs. (20) and (21)] are important. Notice that any periodic solution of the perturbed system (16) and (17) should have the same period (or an integer multiple) as the forcing terms appearing in these equations. Let us assume that we know a periodic solution $\theta(\nu)$, $\varphi(\nu)$ of Eqs. (16) and (17) with period T; for such a solution the left-hand side of those equations are periodic functions of period T. However, in the right-hand side you will find periodic terms with period T mixed with periodic terms of period 2π. In general, the resulting function is not periodic, and the equations do not fulfill unless T would be an integer multiple of 2π. This is the well-known frequency entrainment phenomenon typical of this kind of forced systems.[14]

We did not find periodic solutions with period 4π, 6π, thus, the perturbed system—Eqs. (16) and (17)—only has periodic solutions with the orbital period, which is 2π in terms of the nondimensional variables. So, when $\varepsilon \to 0$, any 2π-periodic solution of Eqs. (16) and (17) approaches a 2π-periodic solution of the unperturbed system, that is, of Eqs. (20) and (21). In summary, all of the periodic solutions of the unperturbed system with period different from 2π will disappear in the perturbed system. On the contrary, each 2π-periodic solution of the unperturbed system ($\varepsilon = 0$) will give place to a family of 2π-periodic solutions of the perturbed system for increasing values of ε.

The equilibrium position 1) is a good example. It is a steady solution of the unperturbed system, and as such, it could be considered periodic with an arbitrary period. If we consider it as a 2π-periodic solution, then, for increasing values of ε, it gives place to a special family of 2π-periodic solutions of the perturbed system, which has been studied in Refs. 11 and 12 using asymptotic techniques [Eqs. (16) of Ref. (12)]. However, apart from this special family there are additional 2π-periodic solutions of the perturbed system as we will show later on in the paper.

Basic Periodic Solution

By using asymptotic techniques, in the limit $\varepsilon_1 \to 0$ the nonlinear Eqs. (16) and (17) have been analyzed in Refs. 11 and 12 to obtain 1) a special family of 2π-periodic solutions, which reduces to the equilibrium position 1) when $\varepsilon = 0$, and 2) their monodromy matrix and the moduli of its eigenvalues λ, which give the stability properties of the 2π-periodic solutions. The procedure used in those papers consists of four stages:

1) First of all, Eqs. (16) and (17) are rewritten in the form

$$\dot{\boldsymbol{x}} = \boldsymbol{F}(\boldsymbol{x}, \nu, \varepsilon_1, i) \tag{23}$$

2) A 2π-periodic solution $\boldsymbol{x}_p$ of these equations is obtained as an asymptotic expansion in powers of the parameter ε_1

$$\boldsymbol{x}_p(\nu, \varepsilon_1, i) \approx \boldsymbol{x}_0 + \varepsilon_1 \boldsymbol{x}_1 + \varepsilon_1^2 \boldsymbol{x}_2 + \cdots \tag{24}$$

3) Perturbing the periodic solution $\boldsymbol{x} = \boldsymbol{x}_p + \boldsymbol{\eta}$, the variational equations of the system (23) are set out:

$$\dot{\boldsymbol{\eta}} = A(\nu, \varepsilon_1, i)\boldsymbol{\eta} \tag{25}$$

Here, A is a square matrix of size 4 with periodic coefficients. (It depends on ν through the periodic solution $\boldsymbol{x}_p$.) The long-term behavior of this linear system is given by the monodromy matrix M associated to the principal matrix of the system (a fundamental matrix $\Phi(\nu)$, which reduces to the unit matrix I when $\nu = 0$, that is, $\Phi(0) = I$). In fact, $M = \Phi(2\pi)$. For the sake of brevity, we refer to this matrix M as the monodromy matrix of the periodic solution $\boldsymbol{x}_p$ involved in the analysis because their eigenvalues determine the stability properties of $\boldsymbol{x}_p$.

4) Using the periodic solution (24), an asymptotic solution of the variational equations (25) is obtained. From such a solution the monodromy matrix M, and its eigenvalues, can be calculated as asymptotic expansions in powers of ε_1

$$M = M_0 + \varepsilon_1 M_1 + \varepsilon_1^2 M_2 + \cdots$$

$$\lambda = \lambda_0 + \varepsilon_1 \lambda_1 + \varepsilon_1^2 \lambda_2 + \cdots$$

This procedure leads to the following expressions of the eigenvalues of the monodromy matrix:

$$\lambda_{1,2} = 1 + (\pi/9)\cot i\, \varepsilon_1^3 \pm j(\pi/6)\cot^2 i\, \varepsilon_1^2 + O\left(\varepsilon_1^4\right) \tag{26}$$

$$\lambda_{3,4} = e^{\pm 2\alpha j}\left[1 \mp \left(\pi\sqrt{3}/18\right)(1 + 4\cot^2 i)\, j\, \varepsilon_1^2 - (\pi/9)\cot i\, \varepsilon_1^3 + O\left(\varepsilon_1^4\right)\right], \qquad \alpha = \pi\sqrt{3} \tag{27}$$

$$|\lambda_{1,2}| = 1 + (\pi/9)\cot i\, \varepsilon_1^3 + O\left(\varepsilon_1^4\right) \tag{28}$$

$$|\lambda_{3,4}| = 1 - (\pi/9)\cot i\, \varepsilon_1^3 + O\left(\varepsilon_1^4\right) \tag{29}$$

taken from Refs. 11 and 12, where j represents the imaginary number.

Propagation in the Parameter ε

We use the numeric algorithm just presented to obtain numerically the exact initial conditions leading to this special family of 2π-periodic solutions and to study their stability. Because the governing Eqs. (16) and (17) have two free parameters ε and i, one of them should be fixed; in this section we fix the inclination i and take ε as the parameter that will be changed. (Here ε plays the role of the parameter σ in the preceding section, where we described the algorithm.)

To start the procedure, we have to know a particular periodic solution, that is, the periodic solution corresponding to a given value ε_a of the parameter that defines the sought-for family. Because we know the asymptotic solution (24) (given in Refs. 11 and 12 up to order ε^5), we select a small value of ε as starting point, for example, $\varepsilon_a = 0.01$, and we use the asymptotic solution (24) to initialize the algorithm.

Then, we increase slightly the value of the parameter up to $\varepsilon_b = \varepsilon_a + \Delta\varepsilon$. The numeric algorithm provides the initial conditions of the 2π-periodic solution corresponding to this new value ε_b and the stability properties of the 2π-periodic solution corresponding to the old value ε_a (in fact, the eigenvalues of the monodromy matrix associated with that periodic solution). Taking this new value ε_b as new starting point and repeating the procedure, we close the loop. Thus, the algorithm provides the family of periodic solutions for increasing ($\Delta\varepsilon > 0$), or decreasing ($\Delta\varepsilon < 0$), values of the parameter.

The algorithm exhibits an interesting property: it improves dramatically the quality of the solution, that is, if the periodicity of the starting solution ε_a is not good, it produces a new solution ε_b whose periodicity is much better.

The results of the propagation carried out in this section are summarized in Figs. 1 and 2. Figure 1b shows the periodic solutions found numerically for $i = 25$ deg and several values of ε, which correspond to $\varepsilon_1 = 0.2$, 0.3, 0.5, 0.7, 0.8, and 0.825. Figure 1a shows the periodic solutions given by the asymptotic analysis in the same cases. For the lowest values of ε, the asymptotic and numeric solutions show a close agreement, but when ε increases the differences become significant, as should be expected. Note that the asymptotic solution overestimates the θ oscillation and underestimates the φ oscillation. The selected value $i = 25$ deg has not a special meaning, that is, the same qualitative behavior is obtained for any other value of i.

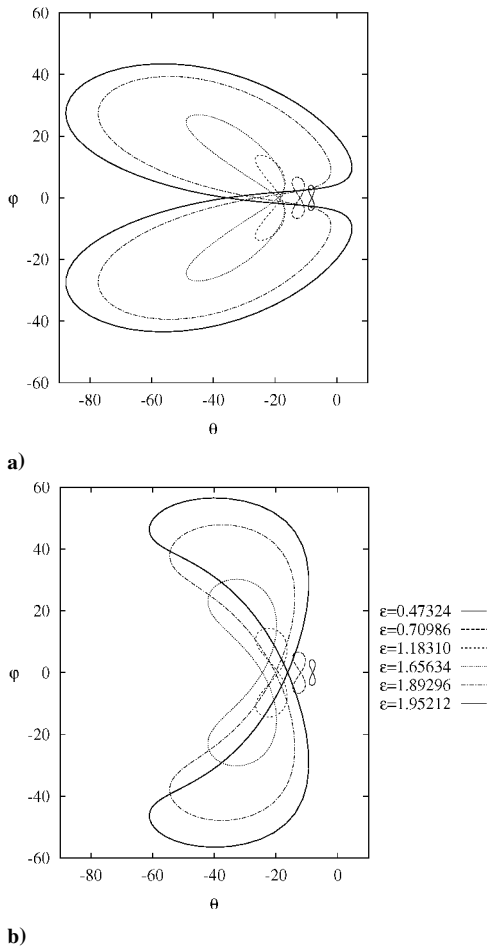

Fig. 1 Periodic solutions given by the a) asymptotic and the b) numeric analysis for $i = 25$ deg and different values of ε: 0.47324, 0.70986, 1.18310, 1.65634, 1.89296, and 1.95212.

In principle, the monodromy matrix of any of these 2π-periodic solutions has four eigenvalues grouped in two pairs of complex conjugate numbers. Figure 2 shows the eigenvalues and their moduli as functions of ε, for two inclinations $i = 25$ and 45 deg. In our calculations many other inclinations have been explored, but in these other cases we obtained the same qualitative behavior; for this reason we selected these values, $i = 25$ and 45 deg, as characteristics of the process that we analyze here. The asymptotic expressions for the eigenvalues [Eqs. (26) and (27)] and the moduli [Eqs. (28) and (29)] rewritten in terms of ε are depicted, as well. Figure 2 shows the excellent behavior of the asymptotic expansions even for values of ε close to unity.

From this analysis some important features should be stressed. First of all, small variations of the modulus of any eigenvalue could give rise to a faster growth of the instability. Thus, if λ changes to $\lambda(1+\delta)$, after n orbits any small initial deviation from the exact periodic solution becomes roughly multiplied by $\lambda^n(1+\delta)^n \simeq \lambda^n(1+n\delta)$, which might be much larger than λ^n. Moreover, if $\lambda = 2$, for example, after $n = 16$ orbits [$\sim$1 day in low Earth orbit], $\lambda^n \simeq 65{,}536$, which is indeed a large number. The eigenvalues $\lambda_{3,4}$ hardly change with the variation of ε and i. However, the eigenvalues $\lambda_{1,2}$ show significant growth for increasing values of the inclination i. Note also, in Fig. 2 the differences between the scales of these eigenvalues in both cases $i = 25$ and 45 deg. As a consequence, when ε is of order unity the instability becomes significant for values of the inclination i, which are not very high.

Figure 2 shows, for $i = 25$ deg, a special value of ε, close to 1.5, for which the moduli of all eigenvalues become equal to one. All of them are imaginary, and so there is no bifurcation to a new periodic orbit. This qualitative behavior appears in our calculation, approximately, when 12 deg $< i <$ 30 deg, and disappears outside that interval (for example, such a special value does not appears for $i = 45$ deg). The system exhibits a neutral stability then, but the analysis is not conclusive in this case. In effect, it would be necessary to retain nonlinear terms in the variational equations to elucidate the stable or unstable character of the periodic solution. However, the correct analysis is not worth, of the effort because the situation we are speaking about is somewhat similar to "the calm before the storm." Shortly after, the complex conjugate eigenvalues $\lambda_{1,2}$ split into two real numbers when ε reaches a critical value ε^*, which is a function of i (which is close to $\varepsilon^* \simeq 1.54$ when $i = 25$ deg in Fig. 2), and the modulus of one of the eigenvalues $\lambda_{1,2}$ increases steeply. Thus, for $\varepsilon > \varepsilon^*$ the instability is strong. The critical value ε^* is a function of the inclination i, which should be numerically calculated.

Figure 3 depicts the function $\varepsilon^* = f(i)$ obtained from the analysis of about 90 different cases. In general, the transition value ε^* is relatively large ($>$1.4), except for high inclinations. When $i \geq 54$ deg, the critical value decreases quickly. For values of i smaller than $\simeq$34 deg, the curve can be fitted by Eq. (30), which was obtained by means of the least-square method and where the inclination i is in degrees. For $i \geq 54$ deg the fitting expression is Eq. (31).

$$\varepsilon^* \simeq 1.40852 + 10^{-3} \cdot i \cdot (1.76703 + i \cdot 0.138841) \quad (30)$$

$$\varepsilon^* \simeq 26.1 - 0.968 \cdot i + 0.0124 \cdot i^2 - 5.37 \cdot 10^{-5} \cdot i^3 \quad (31)$$

Roughly speaking, in the lower region of the plane (ε, i) the instability is weak, and there is a chance to control the tether oscillations by using some damping device. But, when the transition value ε^* is crossed the control becomes much more difficult.

When $\varepsilon < \varepsilon^*$, the modulus of one pair of complex conjugate eigenvalues is always lower than unity. Therefore, the periodic solution has a three-dimensional stable manifold in the state space $(\theta, \varphi, \dot{\theta}, \dot{\varphi}, \nu)$. The other eigenvalues have moduli greater than unity, that is, there is also a three-dimensional unstable manifold that crosses the stable manifold at the periodic solution. Therefore, the destabilization mechanism is the same as the one proposed in Ref. 12.

However, when $\varepsilon > \varepsilon^*$ a qualitative—and quantitative—change takes place in the destabilization mechanism. One of the eigenvalues shows a very significant growth, and, depending on ε and i, one or two additional eigenvalues have moduli greater than unity. As a consequence, the stable manifold shrinks, and for some combinations of i and ε it does disappear (then, the unstable manifold fills the whole state space).

In the propagation process of this family, the parameter ε is bounded, and it increases from zero up to a final value, namely, ε_f. For $i = 25$ deg the value of ε_f is, in approximation, $\varepsilon_f \simeq 1.96$. Beyond this value the family disappears. A transition of the periodic solution from libration to rotation takes place. Figure 1b shows that close to ε_f a small increment of ε causes a significant decrease of the "minimum" value of θ.

Propagation in the Parameter i

For a given value of ε, the numeric algorithm permits the description of the stability properties of the basic periodic solutions after assuming the inclination i as the parameter of the family. To do this, we fix the value of ε, and, starting from $i = 0$ with the asymptotic solution, we propagate the family for increasing values of i. The main results of this analysis are summarized in Figs. 4–6.

Figure 4 shows the moduli of the eigenvalues of the monodromy matrix of the basic periodic solution vs i for different values of ε: 0.2, 0.5, 1.0, and 1.5. First of all, note that the asymptotic expressions given by Eqs. (28) and (29)—dark dashed lines in figure—exhibit a very good behavior even for values of ε close to 1, except for high values of the inclination i. In effect, for a given value of ε and by starting from $i = 0$ deg, the numerical and asymptotic results agree very well, until they reach a critical value of i where both solutions begin to separate. Let i^* be such a critical value that belongs to the curve shown in Fig. 3. For this critical value the complex eigenvalues $\lambda_{1,2}$ split in two real roots, one of which

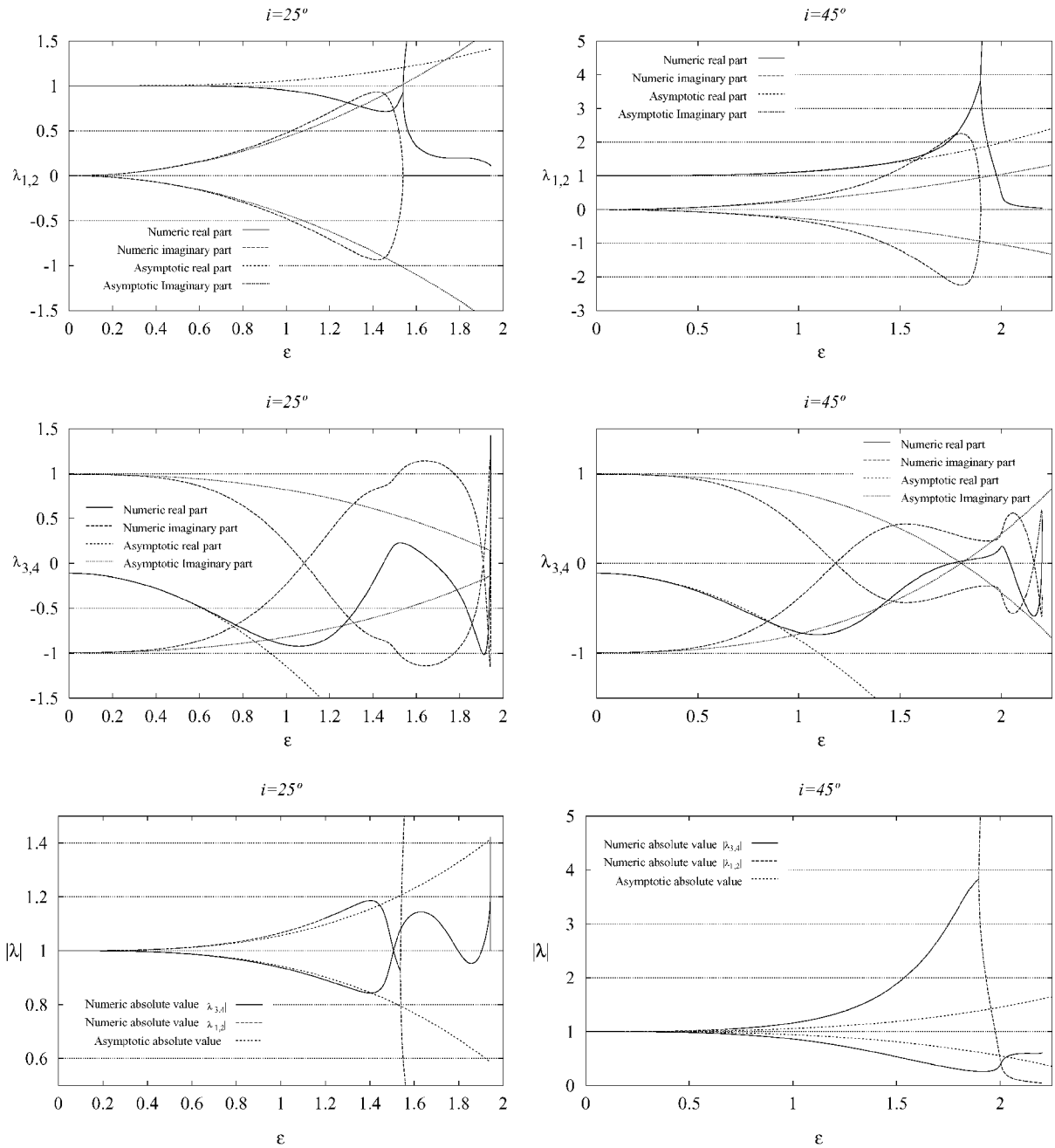

Fig. 2 Eigenvalues of the monodromy matrix vs ε for $i = 25$ and 45 deg.

grows quickly with i (and the numerical results show a strong instability). Note that the difference is very important for ε of order unity. As a consequence, the use of electrodynamic tether on high inclination orbits requires bigger end masses, at first glance, so as to avoid high values of ε. However, this point should be analyzed in more detail because the effectiveness of a vertical electrodynamic tether is small at high inclination orbits, because of the fall of the voltage drop emf produced by the Earth's magnetic field (see Ref. 27).

A closer look shows some interesting features of the family $\mathcal{F}$ of periodic solutions under analysis. After crossing i^*, several bifurcations take place, which change the qualitative behavior of the system. Figure 5 shows, for $\varepsilon = 0.2$ and 0.5, a zoom of Fig. 4 after crossing i^*. For a value of i slightly greater than i^*, one eigenvalue becomes exactly equal to 1, and a new family $\mathcal{F}'$ of periodic solutions appears. The eigenvalues $\lambda_{3,4}$ of the bifurcated family $\mathcal{F}'$ coincide with the eigenvalues $\lambda_{3,4}$ of the original family $\mathcal{F}$, and both agree with the asymptotic solution. However, the eigenvalues $\lambda_{1,2}$ of the bifurcated family $\mathcal{F}'$ are different from the eigenvalues $\lambda_{1,2}$ of the original family $\mathcal{F}$, although they are real as well. After another slight increase of i, the two real eigenvalues $\lambda_{1,2}$ of the bifurcated family $\mathcal{F}'$ become complex again, and, from this point on, the asymptotic solution correctly describes all of the eigenvalues of the bifurcated family $\mathcal{F}'$. For the original family $\mathcal{F}$ the asymptotic solution correctly describes the eigenvalues $\lambda_{3,4}$, but not the eigenvalues $\lambda_{1,2}$, which separate clearly from the asymptotic values.

When the value of ε increases, the asymptotic solution worsens, and the situation becomes more involved. Figure 4 shows the situation for $\varepsilon = 1.0$. For this value the bifurcated family $\mathcal{F}'$, which appears for inclinations greater than $\simeq$58 deg, separates clearly from the asymptotic solution, which is only valid for small values of the inclination i. For $\varepsilon = 1.5$ the asymptotic solution does not describe correctly the behavior of the system even for small values of i. The system response is much more involved, and there are additional bifurcations that appear for small values of i ($\simeq$14 and $\simeq$19 deg) associated with an eigenvalue that also becomes exactly equal to 1. These new bifurcations give rise to new families of periodic orbits that will be studied in the next section. Figure 6 shows two periodic orbits of the original family $\mathcal{F}$ (solid line) and the bifurcated

family $\mathcal{F}'$ (dashed line), which have been obtained for $\varepsilon = 1.0$ and $i = 66$ deg (Fig. 6a) and for $\varepsilon = 1.5$ and $i = 59$ deg (Fig. 6b). The orbits of $\mathcal{F}$ (solid lines) are much more unstable than the orbit of $\mathcal{F}'$.

For larger values of ε, the numeric algorithm experiences difficulties in this attempt to localize periodic solutions.

Finally, we note that the analysis has been focused in a tether working in the generator regime. However, we can take advantage of some invariance properties of the governing equations (16) and (17) to include also the case of a tether working in the thruster mode. In effect, if we introduce the following transformation

$$i \to \pi - i, \qquad \theta \to \theta, \qquad \varphi \to -\varphi, \qquad \varepsilon \to -\varepsilon$$

the relevant equations do not change. Transforming appropriately the initial conditions, we can describe the behavior of the system for negatives values of ε, that is, for the case of a tether working in the thruster mode. Thus, the preceding analysis can be applied to both cases.

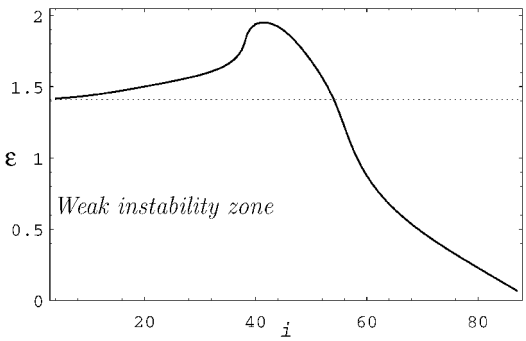

Fig. 3 Critical value ε^* vs i (deg).

Other Periodic Solutions

Apart from the special 2π-periodic solution just analyzed, there are more periodic solutions of the governing equations that we will obtain in this section.

For the unperturbed system the equations governing the small motions around the stable equilibrium (1) can be obtained from Eqs. (20) and (21) through a linearization process. They are

$$\ddot{\theta} + 3\theta = 0 \tag{32}$$

$$\ddot{\varphi} + 4\varphi = 0 \tag{33}$$

and their general solution takes the form:

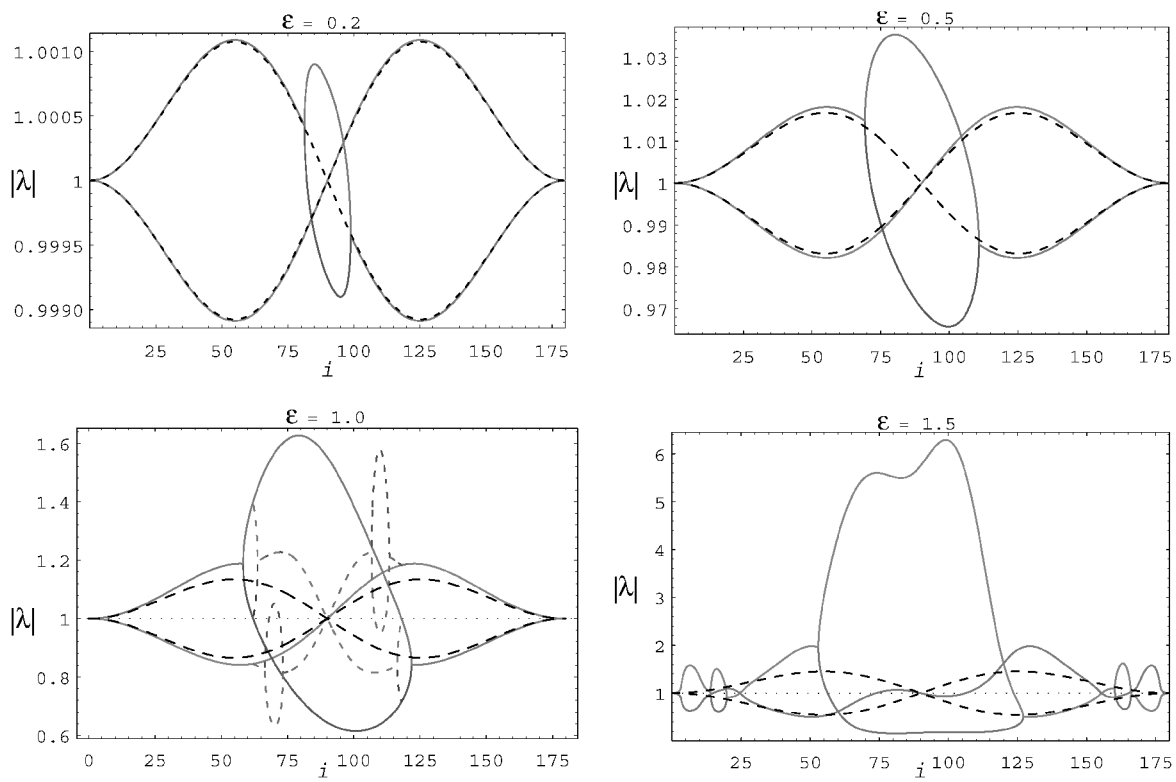

Fig. 4 Moduli of the eigenvalues of the monodromy matrix vs i (deg) for different values of ε.

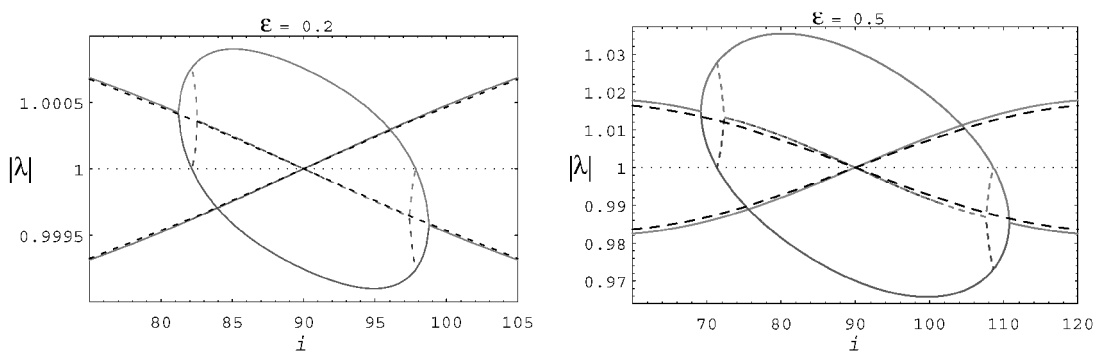

Fig. 5 Original $\mathcal{F}$ and bifurcated $\mathcal{F}'$ families of periodic orbits.

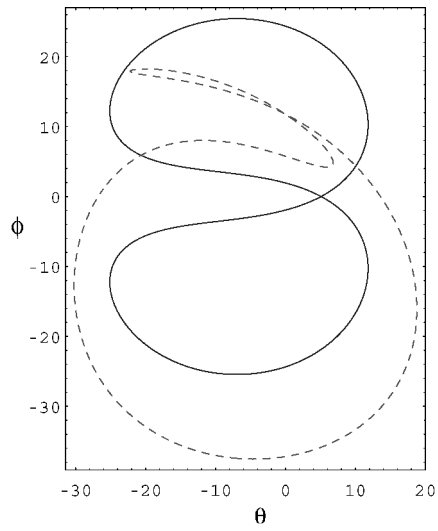

a)

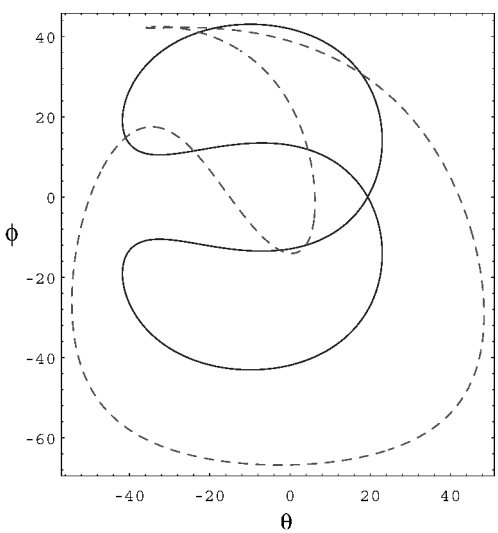

b)

Fig. 6 Orbits of the original family $\mathcal{F}$, ——, and the bifurcated family $\mathcal{F}'$, – – –, a) for $\varepsilon = 1.0$ and $i = 66$ deg and b) for $\varepsilon = 1.5$ and $i = 59$ deg.

$$\theta = A_\theta \cos\left(\sqrt{3}\,\nu + \nu_\theta\right), \qquad \varphi = A_\varphi \cos(2\,\nu + \nu_\varphi)$$

where the amplitudes A_θ, A_φ and the phases ν_θ, ν_φ are arbitrary integration constants. In general, and because of the irrational ratio $2/\sqrt{3}$ between the natural frequencies, the motion will be quasi-periodic but not periodic. However, there are periodic motions associated with the particular solutions:

$$\varphi = 0, \qquad \theta = A_\theta \cos\left(\sqrt{3}\,\nu + \nu_\theta\right) \tag{34}$$

$$\varphi = A_\varphi \cos(2\,\nu + \nu_\varphi), \qquad \theta = 0 \tag{35}$$

Oscillation in θ

In the neighborhood of the equilibrium (1), the eigenvalues of the Hamiltonian system associated with Eqs. (20) and (21) are conjugate complex numbers that take the values

$$-j2,\ -j\sqrt{3}, +j\sqrt{3}, +j2$$

Because the ratio $2/\sqrt{3}$ is irrational, the theory of Hamiltonian system (see Ref. 15, Section 16: An Existence Theorem) states that a family of periodic solutions of the unperturbed system (20) and (21) exists with the following properties: 1) the family depends on one parameter that can be chosen as the amplitude of the oscillation A_θ; 2) the period of the solution depends on the parameter $T = T(A_\theta)$, and when $A_\theta \to 0$ the period approaches $T(0) = 2\pi/\sqrt{3}$; 3) for increasing values of A_θ, the period $T(A_\theta)$ increases; and 4) for small values of A_θ, the family can be approximated by Eqs. (34).

However, for increasing values of A_θ the accuracy of the approximate solution (34) decreases. In this case we have to solve the nonlinear equations (20) and (21). Because $\varphi(\nu) \equiv 0$, they reduce to the following equation:

$$\ddot{\theta} + 3 \sin\theta \cos\theta = 0 \tag{36}$$

which has the energy first integral:

$$\dot{\theta}^2 + 3 \sin^2\theta = 3 \sin^2 A_\theta$$

where the amplitude A_θ is determined by the initial conditions. Because we are looking for periodic solutions, we shift the origin of ν by taking $\sigma = \nu - \nu_1$ as the new independent variable. The phase lag ν_1 is given by the condition: $\theta(\sigma = 0) = 0$. Thus, the nonlinear equation (36) will be integrated from the initial conditions at

$$\sigma = 0: \quad \theta = 0, \qquad \dot{\theta} = \sqrt{3} \sin A_\theta$$

A new integration provides the classical solution

$$\sin\theta = \sin A_\theta \; sn\left(\sqrt{3}\sigma, \sin A_\theta\right) \tag{37}$$

where $sn(\sqrt{3}\sigma, \sin A_\theta)$ is the Jacobian elliptic function with modulus $\sin^2 A_\theta$. The function $sn(u, \sin A_\theta)$ is periodic in u. Its period is $4K(A_\theta)$, where $K(A_\theta)$ is the complete elliptic integral of the first kind:

$$K(A_\theta) = \int_0^{\pi/2} \frac{\mathrm{d}z}{\sqrt{1 - \sin^2 A_\theta \sin^2 z}}$$

$K(A_\theta)$ is a monotonously increasing function. It starts at $K(0) = \pi/2$, and it goes to ∞ for $A_\theta \to \pi/2$. Thus, for a certain value of A_θ, namely, A_θ^*, the oscillation in θ is 2π periodic in σ (and also in the true anomaly). The condition determining A_θ^* is

$$2\pi\sqrt{3} = 4K\left(A_\theta^*\right) \Rightarrow \sin A_\theta^* \simeq 0.9623 \Rightarrow A_\theta^* \simeq 74.217 \text{ deg}$$

Therefore, the 2π-periodic solution found, which corresponds to a libration in the coordinate θ, is

$$\theta = \arcsin\left[\sin A_\theta^* \; sn\left(\sqrt{3}\sigma, \sin A_\theta^*\right)\right] \tag{38}$$

$$\dot{\theta} = \sqrt{3} \sin A_\theta^* \; cn\left(\sqrt{3}\sigma, \sin A_\theta^*\right) \tag{39}$$

$$\varphi = \dot{\varphi} = 0 \tag{40}$$

where $cn(\sqrt{3}\sigma, \sin A_\theta^*)$ is the corresponding Jacobian elliptic function. Figure 7 shows this periodic solution in the phase plane $(\theta, \dot{\theta})$.

The unperturbed problem is autonomous, but the perturbed one is nonautonomous. The periodic solution (38) and (40) can be obtained with many different initial conditions in the variable ν, all of them belonging to the solution (38) and (40). To study the perturbed problem, we must add one more equation in order to obtain an autonomous system, that is, to increase by one the order of the system. In this case the solution (38) and (40) embraces no one but a family of different 2π-periodic solutions in the extended state space. The parameter of such a family is σ. Each one of these 2π-periodic solutions will give rise, after perturbing the parameters ε and/or i, to a new family of 2π-periodic solutions. Thus, arising from the solution (38) and (40) in the perturbed problem there is a family of 2π-periodic solutions with three free parameters: σ, ε, and i.

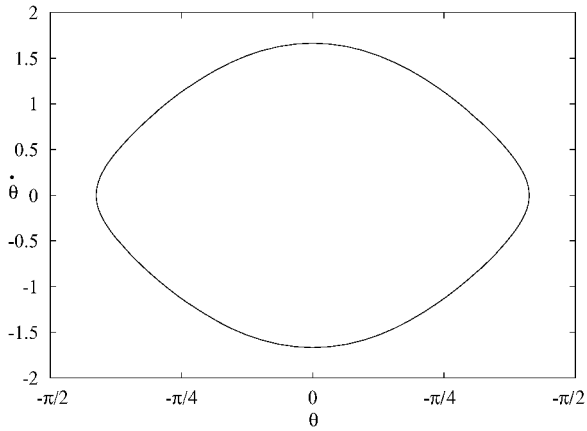

Fig. 7 Oscillation in θ.

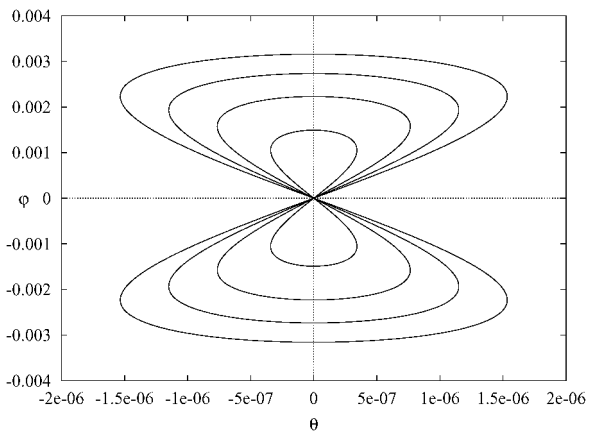

Fig. 8 Oscillation in φ.

Oscillation in φ

We will refer again to the existence theorem of Ref. 15 to show that there is another family of periodic solutions of the unperturbed problem associated with the out-of-plane oscillation (35). Now, the parameter of the family is the amplitude A_φ, and the period of the solutions $T(A_\varphi)$ reaches its minimum value $T(0)=\pi$ at the equilibrium position. For small values of A_φ, the solutions of the family can be approximated by Eq. (35). For increasing values of A_φ, the accuracy of that approximate solution decreases, and we need to take into account nonlinear terms. Introducing the incipient effects of the nonlinear terms, Eqs. (20) and (21) become

$$\ddot{\theta}+3\theta-2\varphi\dot{\varphi}=0, \qquad \ddot{\varphi}+4\varphi+2\varphi\dot{\theta}=0$$

However, if the effects of the nonlinear terms are small the amplitude of the θ oscillation is very small compared with the amplitude of the φ oscillation. Thus, we can simplify the preceding equations by using the approximation $\theta \ll \varphi$, $\dot{\theta} \ll \dot{\varphi}$ to obtain the equations

$$\ddot{\theta}+3\theta-2\varphi\dot{\varphi}=0 \tag{41}$$

$$\ddot{\varphi}+4\varphi=0 \tag{42}$$

which can be easily integrated to get the following periodic solution:

$$\theta=\left(2A_\varphi^2/13\right)\sin 4\sigma, \qquad \varphi=A_\varphi\cos 2\sigma \tag{43}$$

where the independent variable has been appropriately shifted.

Figure 8 shows the periodic solutions of Eqs. (43) for some (small) values of A_φ. These solutions have also been numerically computed starting from small values of A_φ, and using the numeric algorithm we obtain the initial conditions ($\sigma=0$), which lead to the solutions (43). Figure 2 also shows the periodic solutions obtained numerically, which, however, they cannot be distinguished from the approximated solutions (43).

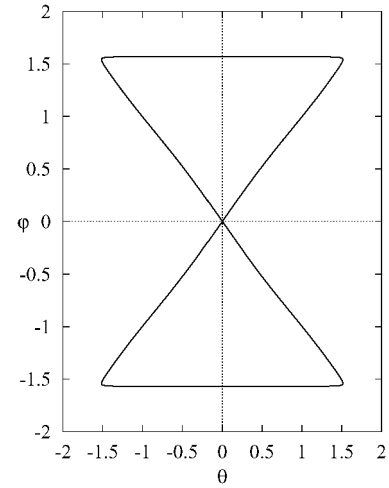

Fig. 9 Numeric limit.

This periodic solution has a constant period for small values of A_φ [see Eqs. (43)]. The period increases with A_φ, and it becomes equal to 2π for a critical value of A_φ. However, before reaching the 2π period the oscillation, which up to this point is a libration, undergoes an important change: turns into a rotation. In effect, the numerical propagation of the family gives $T_{\max}\simeq 4.966$ as the maximum value reached for the period. Figure 9 shows the periodic orbit for this limiting value. For this orbit the maximum value of φ is very close to $\pi/2$, and any further increase of A_φ causes the angle φ to reach $\pi/2$ somewhere along the orbit (that is, solution). The orbit, then, degenerates into a singular point of equations (20) and (21). The numerical continuation of the orbit beyond the singular point it is not possible through the angles θ and φ. In this case it would be necessary to use other generalized coordinates (for example the Euler parameters).

However, for the operation of an electrodynamic tether the 2π-periodic orbit, obtained by propagating the family up to $T=2\pi$, is of little interest. In fact, during a significant fraction of the orbital period the tether would be normal to the orbital plane, and its performances as electron collector would be very poor. This is the reason why we do not study the 2π-periodic orbits of the perturbed problem, which arise from this particular 2π-periodic orbit for increasing values of ε.

Richness of the Unperturbed Problem

Because Eqs. (20) and (21) are strongly nonlinear, the unperturbed problem cannot be integrated analytically. Apart from the 2π-periodic solutions already considered, there are many more solutions with many different periods depending on the initial conditions. Most of them arise at classical bifurcations appearing in the families of periodic orbits. Some of them have periods that are multiple of π, that is, $n\pi$, $n\in\mathbb{Z}$.

Consider, for example, the oscillation in θ given by Eq. (37). The four order monodromy matrix of this periodic orbit is symplectic. If λ is one of its eigenvalues, then $1/\lambda$ is also an eigenvalue. Because the unperturbed problem is autonomous, the periodic orbit has the eigenvalue $\lambda=1$ with multiplicity equal to two. The other two eigenvalues give the stability properties of the orbit, and they are usually summarized in the stability index $k=\lambda_1+\lambda_2$. The solution (37) embraces a family of periodic solutions. The family can be obtained with the help of the numeric algorithm we use in the paper, starting from the solution (34) and propagating over the total energy of the system (or the period). Figure 10 shows the stability index k vs the period P for the orbits of this family described by Eq. (37). Notice that $k=2$ and -2 correspond to bifurcation points of the periodic orbit. In the boundary $k=2$ the periodic orbit becomes unstable. When $k=-2$ is reached, there is a new periodic orbit with two-fold period, that is, we have a flip bifurcation. Figure 10 shows that this new $2P$-periodic solution appears before the period of the family (37) reaches the value 2π [solution (38 and 40)].

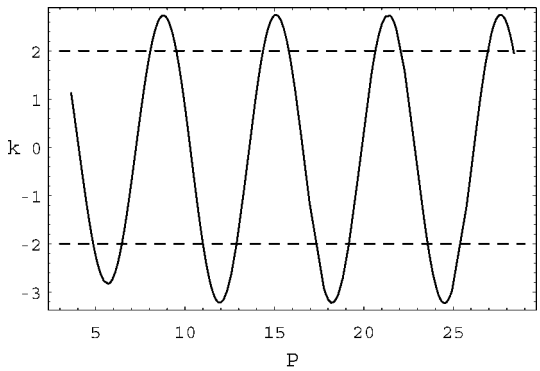

Fig. 10 Stability index k vs period P.

Note, moreover, that when the period P reaches the value 2π the stability index k takes the value $k \simeq -2.327518$, that is, it is lower than -2. In fact, its nontrivial eigenvalues are $\lambda_1 \simeq -1.7590$ and $\lambda_2 \simeq -0.56849$. Therefore, the periodic orbit (38) and (40) is unstable. As a consequence, the family of 2π-periodic solutions arising from Eqs. (38) and (40) after perturbing with the parameters ε and/or i will be, most likely, unstable.

Starting from any one of those bifurcated orbits, and by propagating over the total energy, we will find new bifurcations that give place to more periodic orbits with two-fold period. This is a classic way toward the Hamiltonian chaos. A summary of the situation is given in Fig. 11, which in its center shows a Poincaré section θ–$\dot{\theta}$ ($\varphi = 0, \dot{\varphi} > 0$) obtained for the value $\varepsilon = 1.38906$ of the total energy of the system in the orbital frame, defined (see Refs. 11 and 12) as

$$\varepsilon = \tfrac{1}{2}(\dot{\varphi}^2 + \dot{\theta}^2 \cos^2\varphi) + \tfrac{1}{2}[4 - \cos^2\varphi\,(1 + 3\cos^2\theta)]$$

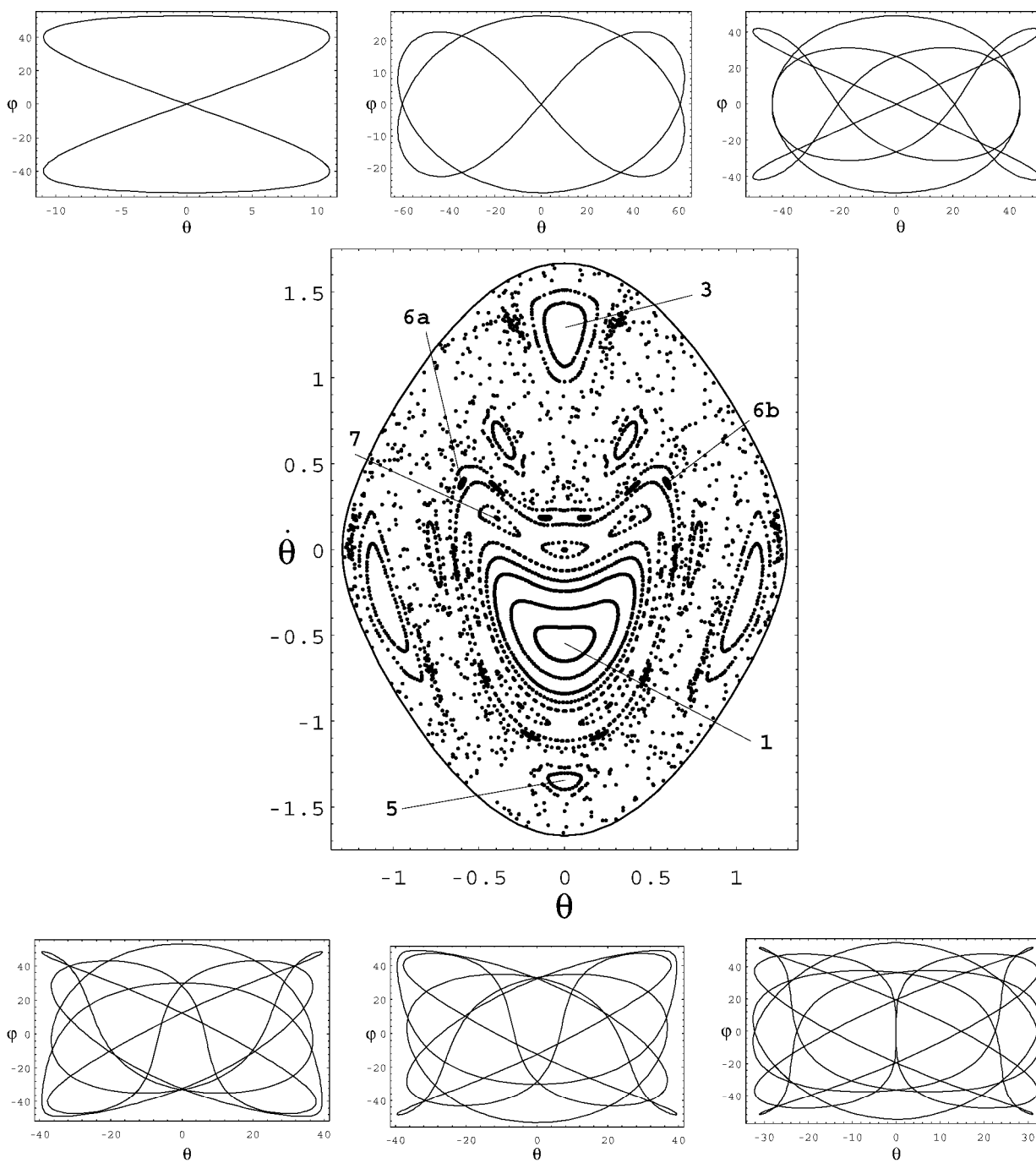

Fig. 11 Poincaré section θ–$\dot{\theta}$ ($\varphi = 0, \dot{\varphi} > 0$) for a total energy of $\varepsilon = 1.38906$ in the orbital frame.

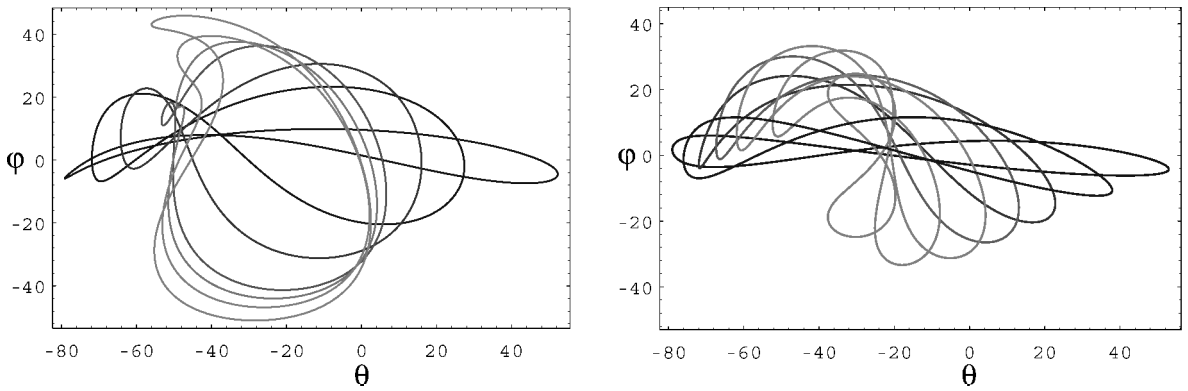

Fig. 12 Periodic orbits of the two families for $i = 25$ deg and different values of ε.

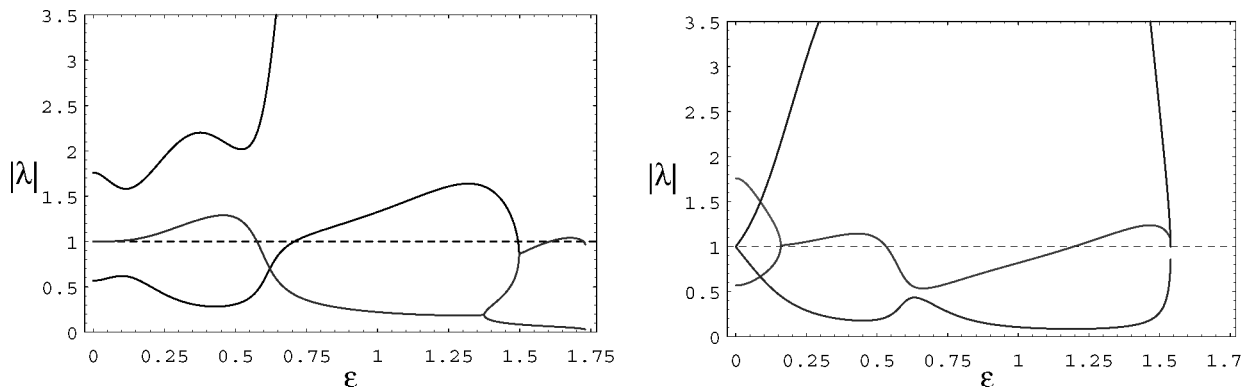

Fig. 13 Moduli of the eigenvalues of the monodromy matrix vs ε for the two families shown in Fig. 12.

Several elliptic points associated with periodic orbits are marked as follows: 1, 3, 5, 6a, 6b, 7. On the top, and from left to right, the figure shows the periodic solution 1 with the fundamental period ($P_1 = 3.647373662059788$), 3 with three-fold period, and 5 with five-fold period. On the bottom, and from left to right, the figure shows two symmetric periodic solutions 6a and 6b with six-fold period and the 7 with seven-fold period.

Aside from the periodic orbits, the picture shows very clearly the stochastic behavior of the system. A more detailed analysis about the nonlinear dynamics of two satellites connected by a rigid tether can be found in Ref. 28.

Propagation for the Other Periodic Solutions

Unlike the basic 2π-periodic solution considered in preceding sections, there is another family of 2π-periodic solution arising from the periodic orbit (38) and (40) of the unperturbed problem. As we already stated, this family of 2π-periodic solutions has three free parameters: σ, ε, and i. In principle, the stability properties of this family can be analyzed with the help of the numeric algorithm propagating anyone of the free parameters. However, the numerical analysis carried out shows that for given values of ε and i there are only four basic cases when σ spans the interval $[0, 2\pi]$. These four families appear in pairs, and, within each pair, one family of periodic orbits is approximately the symmetric of the other family, with respect to the orbital plane. Thus, despite the fact that all of the four families have been studied, we will only present results for two of them. The propagation in the parameter ε has been carried out by fixing the value of the inclination i. We show here the results obtained for $i = 25$ deg. The qualitative behavior is quite similar for other values of i.

Figure 12 shows, when $i = 25$ deg, the periodic orbits of these two families for different values of ε ($\varepsilon = 0.24$, 0.73, 1.08, 1.43, 1.54, 1.65, and 1.73). Note that for small values of ε the orbit is close to a θ oscillation in the orbital plane, but for larger values it is quite different because the out-of-plane motion becomes important.

Figure 13 shows the moduli of the eigenvalues of the monodromy matrix of the periodic solutions for the two families shown in Fig. 12 as functions of ε.

There is always an eigenvalue with modulus greater than one. Therefore, all of the 2π-periodic orbits of both families are unstable. In fact, they are very unstable because the modulus of the critical eigenvalue is larger than two except in a short region where ε is small. This result has been previously guessed at when considering the unstable character of the periodic orbit [Eqs. (38) and (40)] from which they arise. Now, it has been confirmed by the numerical analysis. Both families cannot be propagated beyond a certain value of ε, namely, ε_f. For the family shown in the right-hand-side pictures of the Figs. 12 and 13, $\varepsilon_f \simeq 1.54$. For this value ε_f, the family merges with the basic periodic solution just analyzed. However, for the family shown in the left-hand-side pictures $\varepsilon_f \simeq 1.73$. Despite that, there is no transition from libration to rotation for this value of ε; the propagation beyond this point experiences great difficulties associated with the sharp growth of one of the real eigenvalues.

Conclusions

An electrodynamic tether used to generate thrust is most attractive when operated over long periods of time. However, the long-term operation of this kind of thruster poses some dynamical problems that must be solved. Because the electrodynamic forces prevent the existence of equilibrium position relative to the orbital frame, any periodic solution of the dynamic governing equations is a good starting point for the operation of the tethered system. Such periodic orbits play an important role in the operation of electrodynamic tethers. A detailed analysis of their stability properties, in cases that are relevant to the operation of electrodynamic tethers working in circular inclined orbits, has been carried out.

We use the model described in Refs. 11 and 12. By assuming the tether current constant, only two free parameters appear in the governing equations: the orbital inclination i and ε. The latter gives the order of magnitude of the electrodynamic forces.

The asymptotic analysis of Refs. 11 and 12 has been extended, by tuning a numeric algorithm based on the Poincaré method of continuation of periodic orbits. The algorithm allows the propagation of a family of periodic orbits for different values of any free parameter, starting from a known, particular periodic solution. Using the numeric algorithm, we carried out an analysis as in Refs. 11 and 12, but now for values of ε of order unity, that is, the asymptotic condition $\varepsilon \ll 1$ has been released. We determine the initial conditions leading to the basic periodic solution studied there, and we compare the numeric and the asymptotic solutions. The analysis shows that the asymptotic expressions work very well even for values of ε of order unity, except in two cases: 1) in the neighborhood of $i = 90$ deg and 2) for high values of ε. High inclination orbits are not appropriate, at first sight, for the operation of a vertical electrodynamic tether. For a tether working in the generator mode, for example, the collection of electrons from the ionosphere becomes more difficult because of the fall of the voltage drop emf generated by the Earth magnetic field. However, to elucidate this point it would be necessary to give a more detailed analysis that considers the variation of the tether current I_m with the voltage drop emf, that is, with the angles θ and φ (see Ref. 27).

The analysis shows that for a given inclination there is a critical value ε^* of the electrodynamic forces beyond which the destabilizing mechanism becomes very powerful because one of the eigenvalues of the monodromy matrix grows very quickly when $\varepsilon > \varepsilon^*$. We estimated, numerically, the boundary $\varepsilon^* = f(i)$. Approximated expressions for this critical value [see Eqs. (30) and (31)] have been obtained for small and large values of i, as well. From the point of view of the operation of an electrodynamic tether, it appears convenient to operate the tether away from that threshold during most of the time. For $\varepsilon < \varepsilon^*$ the instability could be controllable with the help of dumping or tether current modulation. However, when $\varepsilon > \varepsilon^*$ the control of the system will be more difficult because the instability is stronger.

Finally, we show that there are more periodic solutions of the governing equations. At first sight they could be used as a starting point for the operation of the electrodynamic tether. The numeric algorithm yields these additional periodic solutions and their stability properties. Unfortunately, all of them are unstable; in fact, they are more unstable than the basic periodic solution studied in Refs. 11 and 12 and in this paper. As a consequence, they are not appropriate for the long-term operation of the electrodynamic tether.

Acknowledgments

The work of J. Peláez was carried out in the framework of the research project entitled "Dinámica de "Tethers" Electrodinámicos" supported by the Dirección General de Enseñanza Superior e Investigación Científica of the Spanish Ministry of Education (PB97-0574-C04-04). The authors thank Enrico C. Lorenzini for the tedious task of revising the English of the manuscript. His fruitful comments contributed greatly to the improvement of the final version of the paper.

References

[1]Banks, P. M., Willimason, P. R., and Oyama, K., "The Electrodynamic Tether," Rept. NAS5-23837, *UAH/NASA Workshop on the Use of a Tethered Satellite System*, edited by S. T. Wu, NASA, Huntsville, AL, May 1978, pp. 163–175.

[2]Colombo, G., Grossi, M. D., Dobrowolny, M., and Arnold, D. A., "Electrodynamic Stabilization and Investigation of Electrodynamic Statilization and Control of Long Orbiting Tethers," NASA CR NAS8-33691, Aug. 1980.

[3]Martínez-Sánchez, M., and Hastings, D. V., "A System Study of a 100 KW Electro-Dynamic Tether," *The Journal of the Astronautical Sciences*, Vol. 35, No. 1, 1987, pp. 75–96.

[4]Sanmartín, J. R., Martínez-Sánchez, M., and Ahedo, E., "Bare Wire Anodes for Electrodynamic Tether," *Journal of Propulsion and Power*, Vol. 9, No. 3, 1993, pp. 353–360.

[5]Johnson, L., and Ballance, J., "Propulsive Small Expendable Deployer System (ProSEDS) Space Demonstration," *Space Technology and Applications International Forum 1998*, Vol. 420, No. 1, Jan. 1998, pp. 354–358.

[6]Johnson, L., Estes, R. D., Lorenzini, E., Martínez-Sánchez, M., and Sanmartín, J., "Propulsive Small Expandable Deployer System Experiment," *Journal of Spacecraft and Rockets*, Vol. 37, No. 2, 2000, pp. 173–177.

[7]Estes, R. D., Lorenzini, E. C., Sanmartín, J. R., Peláez, J., Martínez-Sánchez, M., Johnson, L., and Vas, I., "Bare Tethers for Electrodynamic Spacecraft Propulsion," *Journal of Spacecraft and Rockets*, Vol. 37, No. 2, 2000, pp. 205–211.

[8]Vass, I. E., Kelley, T. J., and Scarl, E. A., "Space Station Reboost with Electrodynamic Tethers," *Journal of Spacecraft and Rockets*, Vol. 37, No. 2, 2000, pp. 154–164.

[9]Levin, E. M., "Stability of the Stationary Motions of an Electrodynamic Tether System in Orbit," *Cosmic Research*, Vol. 25, July–Aug. 1987, pp. 368–376.

[10]Beletskii, V. V., and Levin, E. M., *Dynamics of the Space Tether System*, Advances in the Astronautical Sciences, Vol. 83, Univelt, San Diego, CA, 1993, pp. 268–322.

[11]Peláez, J., Lorenzini, E. C., López-Rebollal, O., and Ruiz, M., "A New Kind of Dynamic Instability in Electrodynamic Tethers," *Spaceflight Mechanics 2000*, Advances in the Astronautical Sciences, Vol. 105, Univelt, San Diego, CA, 2000, pp. 1367–1386.

[12]Peláez, J., Lorenzini, E. C., López-Rebollal, O., and Ruiz, M., "A New Kind of Dynamic Instability in Electrodynamic Tethers," *The Journal of the Astronautical Sciences*, Vol. 48, No. 4, 2000, pp. 449–476.

[13]Peláez, J., Ruiz, M., López-Rebollal, O., Lorenzini, E. C., and Cosmo, M. L., "A Two Bar Model for the Dynamics and Stability of Electrodynamic Tethers," *Spaceflight Mechanics 2000*, Advances in the Astronautical Sciences, Vol. 105, Univelt, San Diego, CA, 2000, pp. 1327–1346.

[14]Murdock, J. A., *Perturbations: Theory and Methods*, Classics in Applied Mathematics, Wiley, New York, 1991.

[15]Siegel, C. L., and Moser, J. K., *Lectures on Celestial Mechanics*, Classics in Mathematics, Springer-Verlag, Berlin, 1971.

[16]Baranger, M., Davies, K. T. R., and Mahoney, J. H., "The Calculation of Periodic Trajectories," *Annals of Physics*, Vol. 186, No. 1, 1988, pp. 95–110.

[17]Deprit, A., and Henrard, J., "Natural Families of Periodic Orbits," *Astronomical Journal*, Vol. 72, No. 2, 1967, pp. 158–172.

[18]Howell, K. C., "Three-Dimensional, Periodic 'Halo' Orbits," *Celestial Mechanics*, Vol. 32, No. 1, 1984, pp. 53–71.

[19]Karimov, S. R., and Sokolsky, A. G., "Periodic Motions Generated by Lagrangian Solutions of the Circular Restricted Three-Body Problem," *Celestial Mechanics*, Vol. 46, No. 4, 1989, pp. 335–381.

[20]Belbruno, E., Llibre, J., and Olle, M., "On the Families of Periodic Orbits Which Bifurcate from the Circular Sitnikov Motions," *Celestial Mechanics and Dynamical Astronomy*, Vol. 60, No. 1, 1994, pp. 99–129.

[21]Simonovic, N. S., "Calculation of Periodic Orbits: the Monodromy Method and Application to Regularized Systems," *Chaos*, Vol. 9, No. 4, 1999, pp. 854–864.

[22]Lara, M., "Un Algoritmo para la Continuación Analítica de Órbitas Periódicas," *Monografías del Seminario Matemático "García de Galdeano,"* Vol. 21, 2001, pp. 11–20.

[23]Lara, M., and Peláez, J., "On the Numerical Continuation of Periodic Orbits: An Intrinsic, 3-Dimensional, Differential, Predictor-Corrector Algorithm," *Astronomy and Astrophysics*, Vol. 389, No. 2, 2002, pp. 692–701.

[24]Szebehely, V., *Theory of Orbits—The Restrictec Problem of Three Bodies*, Academic Press, New York, 1967, Chap. 8.

[25]Lara, M., "Searching for Repeating Ground Track Orbits: A Systematic Approach," *The Journal of the Astronautical Sciences*, Vol. 47, No. 3–4, 1999, pp. 177–188.

[26]Guckenheimer, J., and Holmes, P., *Nonlinear Oscillations, Dynamical Systems, and Bifurcations of Vector Fields*, 3rd ed., *Applied Mathematical Sciences*, Vol. 142, Springer-Verlag, New York, 1983, pp. 25, 26.

[27]Peláez, J., López-Rebollal, O., Lara, M., and Ahedo, E. "Dynamic Stability of a Bare Tether as a Deorbiting Device," *Spaceflight Mechanics 2002*, Advances in the Astronautical Sciences, Vol. 112, Univelt, San Diego, CA, 2002, pp. 1257–1274.

[28]Misra, A. K., Nixon, M. S., and Modi, V. J., "Nonlinear Dynamics of Two-Body Tethered Satellite Systems: Constant Length Case," *The Journal of the Astronautical Sciences*, Vol. 49, No. 2, 2001, pp. 219–236.